

1 **Non-negligible secondary contribution to brown carbon in autumn and winter:**
2 **inspiration from particulate nitrated and oxygenated aromatic compounds in**
3 **urban Beijing**

4
5
6 Yanqin Ren¹, Zhenhai Wu¹, Yuanyuan Ji¹, Fang Bi¹, Junling Li¹, Haijie Zhang¹, Hao
7 Zhang¹, Hong Li^{1*}, Gehui Wang^{2*}

8
9 ¹ State Key Laboratory of Environmental Criteria and Risk Assessment, Chinese
10 Research Academy of Environmental Sciences, Beijing 100012, China

11 ² Key Lab of Geographic Information Science of Ministry of Education of China,
12 School of Geographic Sciences, East China Normal University, Shanghai 200142,
13 China

14
15
16 *Corresponding authors: Dr. Gehui Wang/ Dr. Hong Li

17 E-mail address: ghwang@geo.ecnu.edu.cn / lihong@craes.org.cn

18 **Abstract**

19 Nitrated aromatic compounds (NACs) and oxygenated derivatives of polycyclic
20 aromatic hydrocarbons (OPAHs) play vital roles within brown carbon (BrC),
21 influencing both climate dynamics and human health to a certain degree. The
22 concentrations of these drug classes were analyzed in PM_{2.5} from an urban area in
23 Beijing during the autumn and winter of 2017 and 2018. There were four heavy haze
24 episodes during the campaign; two of which happened prior to heating whereas the
25 other two during heating. During the entire course of sampling, the mean total
26 concentrations of the nine NACs and the eight OPAHs were 1.2-263 and 2.1-234 ng m⁻³,
27 respectively. The concentrations of both NACs and OPAHs were approximately 2-3
28 times higher in the heating period than before heating. For NACs, the relative molecular
29 composition did not change significantly before and during heating, with 4-
30 nitrocatechol and 4-nitrophenol demonstrating the highest abundance. For OPAHs, 1-
31 Naphthaldehyde was the most abundant species before and during heating, while the
32 relative proportion of Anthraquinone increased by more than twice, from 13% before
33 heating to 31% during the heating. In Beijing's urban area during autumn and winter,
34 significant sources of NACs and OPAHs have been traced back to automobile emissions
35 and biomass burning activities. Interestingly, it was observed that the contribution from
36 coal combustion increased notably during heating. It is worth noticing that the
37 secondary generation of BrC was important throughout the whole sampling period,
38 which was manifested by the photochemical reaction before heating and the aqueous

39 reaction during heating. It was further found that the haze in autumn and winter was
40 nitrate-driven before heating and SOC-driven during heating, and the secondary
41 formation of BrC increased significantly in pollution events, particularly during heating.

42 **1 Introduction**

43 As an important light-absorbing material, brown carbon (BrC) has garnered
44 increasing attention in recent years (Jiang et al., 2023; Song et al., 2022; Zhang et al.,
45 2021b; Liu et al., 2023; Ren et al., 2023; Ren et al., 2022; Chen et al., 2022). BrC could
46 not only directly absorb solar energy, but also indirectly contribute to climate change
47 by promoting the evaporation of water and the dispersal of clouds (Laskin et al., 2015;
48 Huang et al., 2018). BrC also has potential adverse effects on human health on account
49 of its strong mutagenic, cytotoxic, and carcinogenic properties (Teich et al., 2016).

50 Primary as well as secondary sources contribute to the atmospheric accumulation
51 of BrC (Zhu et al., 2021). Direct emissions of primary BrC come from burning biomass
52 and combustion of fossil fuels (Ni et al., 2021; Wang et al., 2020a; Lu et al., 2019a; Lu
53 et al., 2019b). Secondary BrC in the atmosphere is produced from oxidation and aging
54 processes (Wang et al., 2019; Wang et al., 2020c; Cheng et al., 2021; Jiang et al., 2023;
55 Cai et al., 2022). Toluene, phenol, benzene, and other aromatic hydrocarbons can be
56 oxidized to produce nitrophenol or nitrocatechol by NO_3 or OH radical vapor phase in
57 the presence of NO_x (Olariu et al., 2002; Sato et al., 2007; Iinuma et al., 2010; Ji et al.,
58 2017). VOCs can be oxidized to produce nitro-aromatic hydrocarbons when emitted

59 during biomass combustion and pyrolysis (such as cresol, catechol, methyl catechol,
60 etc.) (Iinuma et al., 2010; Claeys et al., 2012; Finewax et al., 2018). Research on the
61 source analysis of brown carbon (BrC) frequently focuses on examining two key
62 constituents: the carbon component within humic-like substances (HULIS-C) and
63 water-soluble organic carbon (WSOC). These components are often studied to
64 understand the origins and properties of BrC in various environmental contexts.
65 Secondary generation and burning of biomass are the two main sources of HULIS in
66 Guangzhou and Shanghai (Fan et al., 2016; Zhao et al., 2016). In comparison with the
67 water-insoluble BrC in the winter, the contribution of non-fossil sources (for instance
68 burning biomass) to water-soluble BrC was sometimes as high as 70% or more (Liu et
69 al., 2018; Song et al., 2018). Coal combustion is presumably a significant source of
70 HULIS in the winter, in addition to burning biomass and secondary generation (Tan et
71 al., 2016). According to multiple studies conducted in Beijing, the primary contributor
72 to WSOC is secondary generation, accounting for 54% of its composition. Following
73 this, biomass burning contributes approximately 40%, while other primary emission
74 sources contribute a smaller proportion, making up only 6% (Du et al., 2014). In Beijing,
75 the percentages of biomass burning, coal combustion, and secondary generation that
76 contribute to atmospheric HULIS are 47%, 15%, and 39%, respectively. The primary
77 origins of HULIS show minimal association with motor vehicles and industrial
78 emissions (Li et al., 2019). According to Ma et al. (2018), secondary generation is
79 responsible for over 50% of HULIS in the non-heating season. Biomass burning
80 represents 21% of the HULIS content during this period. However, in the heating

81 season, approximately 40% of HULIS originates from biomass burning, while the
82 remaining 60% is contributed by diverse combustion sources like coal burning, waste
83 incineration, and vehicular emissions. Within this season, secondary generation
84 accounts for about 19% of the HULIS content (Ma et al., 2018).

85 The research suggests that various sources contribute to BrC, but their relative
86 impact varies depending on time and location. As a result, the chemical makeup, light
87 absorption characteristics, and concentrations of BrC show considerable variability.
88 This variability poses challenges in accurately assessing and forecasting the influence
89 of these sources on radiation and climate changes (Wang et al., 2020b; Yan et al., 2018;
90 Laskin et al., 2015). However, until recently, there was only a limited volume of
91 research pertaining to the sources and pathways of BrC leading to their generation in
92 the densely populated city environment. NACs and OPAHs are the primary focus of
93 this study because several studies have noted that nitrogen-containing aromatics,
94 polycyclic aromatic hydrocarbons (PAHs), and their derivatives are significant BrC
95 chromophores (Huang et al., 2018; Wu et al., 2020; Liu et al., 2023; Wang et al., 2020b;
96 Xie et al., 2017). The average contribution of OPAHs (five species) to the solar-
97 spectrum weighed absorption coefficient of water-insoluble BrC in summer is
98 $0.51 \pm 0.28\%$ during daytime and $0.34 \pm 0.19\%$ during nighttime. The contribution of
99 NACs to light absorption of water-soluble BrC is on average 2.5 times higher during
100 nighttime ($3.47 \pm 2.03\%$) than during the day ($1.41 \pm 0.29\%$) in winter, and the fractions
101 are much higher in winter than in summer ($0.12 \pm 0.03\%$) (Li et al., 2020a). It is well-
102 established that residential heating plays a significant role in the substantial increase of

103 anthropogenic pollutant emissions during the winter season. There is a substantial rise
104 in the emission of aromatics-derived secondary organic aerosol from autumn to winter
105 (Ding et al., 2017), and particle BrC is often detected especially in haze periods (Liu et
106 al., 2023). This study was conducted in the autumn and winter of 2017 and 2018 in
107 Beijing. Nine NACs and eight OPAHs were measured in PM_{2.5} samples, with a focus
108 on examining their sources, compositions, and concentration variations under various
109 air conditions. Specifically, emphasis was placed on investigating the contribution of
110 secondary generation to these two typical BrC species, particularly their involvement
111 in particle pollution processes during autumn and winter.

112 **2 Materials and Methods**

113 **2.1 Field observations**

114 PM_{2.5} was sampled at a height of 10m on the rooftop of a building at the Chinese
115 Research Academy of Environmental Sciences (CRAES), Beijing, China (40°02'N,
116 116°24'E). Using a high-volume sampler (1.13 m³ min⁻¹, Thermofisher Co., USA),
117 PM_{2.5} specimens were collected in the autumn and winter of 2017 and 2018. The
118 sampling process was executed from 8:00 to 19:30 during the day and from 20:00 to
119 7:30 in the subsequent morning. The specimens and blanks were gathered using a pre-
120 combusted quartz fiber filter (at 450 °C for 6 h). A total of 4 field blanks and 122 PM_{2.5}
121 samples were acquired. Individual filters were sealed in a bag made from an aluminum
122 foil bag before sampling and analysis and placed in a freezer set at a temperature of -

123 20 °C.

124 Using automatic equipment (CRAES Supersite for Comprehensive Urban Air
125 Observation and Research), meteorological parameters such as air temperature (T, °C)
126 and relative humidity (RH, %) along with gaseous pollutants (SO₂, NO₂, O₃, and CO)
127 were observed and measured at the same time.

128 **2.2 Chemical analysis**

129 The present study employed a pre-treatment comprising ultrasonic extraction and
130 derivatization in an attempt to analyze the organic species in the specimens. The details
131 of specimen extraction and derivatization have already been published (Wang et al.,
132 2009; Ren et al., 2021; Ren et al., 2023). In brief, filter aliquots were sectioned and
133 extracted with a methanol and dichloromethane (1:2 v/v,) mixture. Following the
134 concentration of the extracts to dryness, derivatization was carried out using a mixture
135 of N, O-bis-(trimethylsilyl) trifluoroacetamide [BSTFA+TMCS, (99:1), v/v] and
136 pyridine (5:1, v/v). Lastly, the derivatized samples were examined using gas
137 chromatography coupled with a mass spectroscopy detector (GC/MS: HP 7890A, HP
138 5975C, Agilent Co., USA). The extraction and derivatization methods described above
139 allowed for the simultaneous measurement of the samples' polar and non-polar
140 constituents.

141 Given that OPAHs and NACs were the main points of focus, this study
142 investigated a total of eight OPAHs and nine NACs. The nine NACs included 2,4-
143 dinitrophenol (2, 4-DNP), 4-nitrophenol (4NP), 3-methyl-4-nitrophenol (3M4NP), 4-
144 nitrocatechol (4NC), 4-methyl-5-nitrocatechol (4M5NC), 4-nitroguaiacol (4NGA), 5-

145 nitroguaiacol (5NGA), 3-nitro-salicylic acid (3NSA), and 5-nitro-salicylic acid (5NSA),
146 while the eight OPAHs encompassed 9-fluorenone (9-FO), benzanthrone (BZA), 1-
147 Naphthaldehyde (1-NapA), anthraquinone (ATQ), 1,4-chrysenequione (1,4-CQ),
148 benzo(a)anthracene-7,12-dione (7,12-BaAQ), 5,12-naphthacenequione (5,12-NAQ)
149 and 6H-benzo(cd)pyrene-6-one (BPYRone).

150 The elemental carbon (EC) and organic carbon (OC) content of individual PM_{2.5}
151 filter samples were analyzed using an Atmoslytic Inc. DRI model 2001 Carbon
152 Analyzer. This analysis followed the Interagency Monitoring of Protected Visual
153 Environments (IMPROVE) thermal/optical reflectance (TOR) protocol, involving the
154 examination of a 0.526 cm² punch from each specimen. The specifics of the above-
155 described techniques have been documented in literature (Li et al., 2016; Ren et al.,
156 2021).

157 **2.3 Evaluation of secondary BrC**

158 In this study, the contributions of secondary oxidation to the detected NACs and
159 OPAHs were evaluated by using a CO-tracer method, which is comparable to the EC-
160 tracer used for secondary OC quantification. Various methodologies have been
161 similarly adopted successfully in other studies (Liu et al., 2023; Cai et al., 2022).
162 Equation 1 and Equation 2 were respectively used to evaluate the secondary formation
163 of NACs and OPAHs.

$$164 \quad [\text{NACs}]_s = [\text{NACs}]_t - ([\text{NACs}]_t / [\text{CO}])_{\text{pri}} \times [\text{CO}] \quad (1)$$

$$165 \quad [\text{OPAHs}]_s = [\text{OPAHs}]_t - ([\text{OPAHs}]_t / [\text{CO}])_{\text{pri}} \times [\text{CO}] \quad (2)$$

166 [NACs]_s and [NACs]_t in Equation 1 refer to the NACs concentration produced by

167 secondary oxidation and the total amount of NACs, respectively. $([\text{NACs}] / [\text{CO}])_{\text{pri}}$
168 represents the primary emission ratio of NACs in relation to combustion. This
169 calculation assumes that the primary source was predominant during the period, with
170 minimal secondary production. The $([\text{NACs}] / [\text{CO}])_{\text{pri}}$ was calculated in this work by
171 fitting the 15% lowest $[\text{NACs}]_t / [\text{CO}]$ ratios observed during the entire sampling
172 duration. In equation 2 the concentration of OPAHs produced by secondary oxidation
173 and the total observed OPAHs are denoted by $[\text{OPAHs}]_s$ and $[\text{OPAHs}]_t$ respectively.
174 The concentration of CO is denoted by $[\text{CO}]$, while the primary emission ratio of
175 OPAHs in relation to combustion is represented by $([\text{OPAHs}] / [\text{CO}])_{\text{pri}}$, which was
176 calculated by fitting the lowest 15% $[\text{OPAHs}]_t / [\text{CO}]$ ratios observed in the entire
177 sample interval.

178 **3 Results and discussion**

179 **3.1 Variations in major components of PM_{2.5} with respect to meteorological** 180 **conditions and gaseous pollution**

181 Based on the Beijing heating time, the entire period of the study was divided into
182 two phases: before heating (18 October to 14 November 2017) and during heating (15
183 to 23 November 2017; 23 December 2017 to 17 January 2018). Table 1 and Fig. 1
184 present the temporal fluctuations in meteorological factors, gaseous pollutant
185 concentrations, and the main PM_{2.5} components in the two phases. The temperature (T)
186 and relative humidity (RH) were higher before heating (11 ± 3.8 °C and $49 \pm 26\%$) than

187 during heating (1.9 ± 4.4 °C and $23 \pm 15\%$), with average values amounting to $5.9 \pm$
188 5.9 °C and $35 \pm 25\%$, respectively. SO₂ concentrations during heating (4.3 ± 1.5 ppb)
189 were more than twice that before heating (2.1 ± 0.8 ppb), presumably because of the
190 increase in household coal burning for heating. The levels of NO₂ and NO remained
191 consistent before and during heating, suggesting that these pollutants were minimally
192 impacted by heating and were primarily influenced by mobile sources in Beijing. This
193 pattern seems to remain stable in the short term.

194 Fig.2 shows the variation in the chemical makeup of PM_{2.5} in the whole sampling
195 period, before and during heating, respectively. Secondary inorganic aerosols (SIA, i.e.
196 SO₄²⁻, NH₄⁺, and NO₃⁻) were identified as the leading constituents of PM_{2.5}, followed
197 by OM (1.6 times OC), with an average of 31.5% and 20.4% in the whole sampling,
198 respectively (Fig. 2a). Even though the PM_{2.5} concentrations remained relatively stable
199 during this period (as indicated in Table 1 and Fig. 2), there were significant changes
200 observed in the concentrations of SIA and OM, as well as their relative contributions to
201 PM_{2.5}. SIA accounted for 41.9% of PM_{2.5} before heating, which notably decreased to
202 23.1% during heating. This decline was primarily evident in the reduction of NO₃⁻.
203 SO₄²⁻, NO₃⁻, and NH₄⁺ were measured at 5.5, 16, and 5.4 μg m⁻³, respectively, with
204 constituted 8.7%, 24.7%, and 8.5% of PM_{2.5} before heating (Fig. 2b). And their
205 concentrations decreased to 4.3, 6.8, and 4.2 μg m⁻³ (Table 1). The relative contributions
206 of NO₃⁻ to PM_{2.5} dropped dramatically to 10.3% during heating, amounting to a drop
207 of nearly 60%. Both SO₄²⁻ and NH₄⁺ experienced a roughly 25% decrease in their
208 relative contributions to PM_{2.5}, as illustrated in Fig. 2c. The relative abundance of OM

209 to PM_{2.5} increased from 18.6% before heating to 21.9% during heating, with the average
 210 mass concentration of OC showing an increase from 7.4 to 9.1 $\mu\text{g m}^{-3}$ in the
 211 corresponding duration. The OC/EC ratio also increased by 63% from 2.7 ± 3.3 before
 212 heating to 4.4 ± 3.7 during heating. These significant changes in SIA and OM, including
 213 concentrations and the relative contributions to PM_{2.5}, showed that primary organic
 214 aerosols and/or VOCs emissions were the leading contributors during the heating
 215 seasons due to household heating (Tan et al., 2018). It is important to note that the
 216 decrease proportion of SIA in PM_{2.5} may also be affected by meteorological conditions
 217 during heating, which often influencing their production (Wang et al., 2016; An et al.,
 218 2019). For example, increased sulfate is often accompanied by a high RH in the urban
 219 atmosphere and the reaction rate of nitrate formation is accelerated by increasing RH
 220 (Zhang et al., 2015; Sun et al., 2013). However, the RH were lower during than before
 221 heating. Aside from coal combustion, the rise in mass concentrations of K⁺ and Cl⁻
 222 indicated additional burning activities occurring during heating, such as biomass
 223 burning (Bai et al., 2023; Li et al., 2022).

Table 1. Gaseous pollution concentrations and meteorological parameters and chemical constituents of PM_{2.5} during the sampling periods in Beijing.

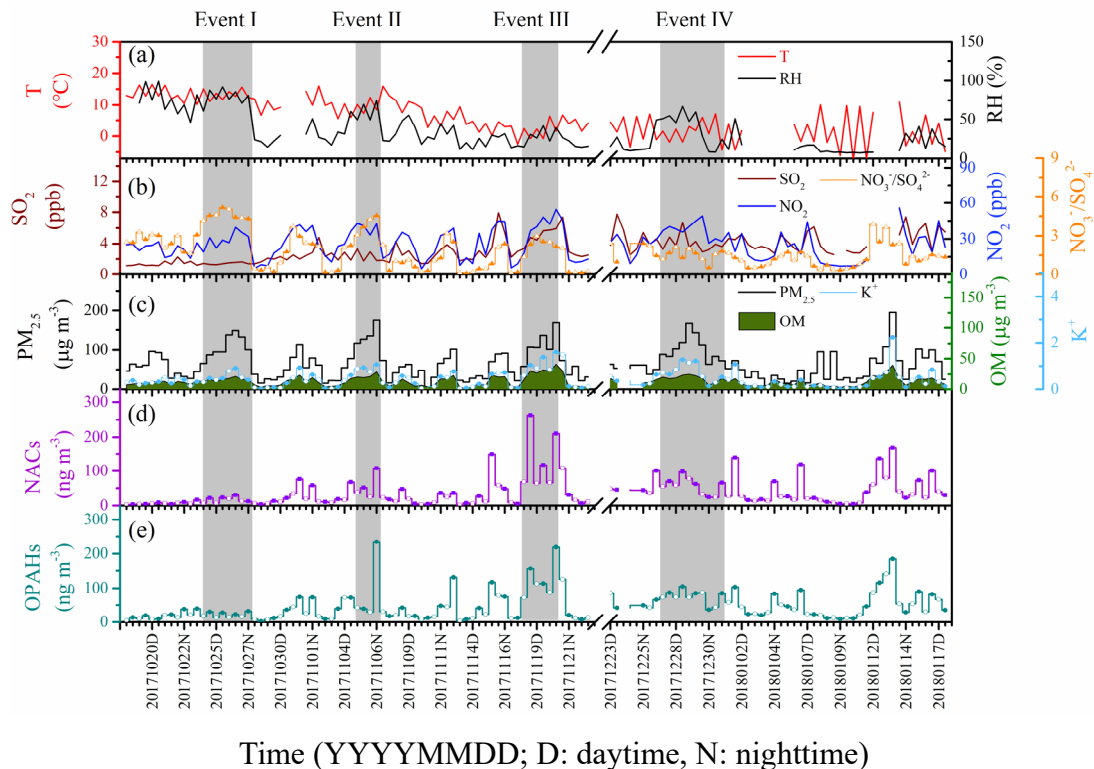
	The whole sampling <i>N</i> =122	Before heating period 18/10–14/11, 2017 <i>N</i> =56	During heating period 15/11–23/11, 2017 23/12, 2017–17/1, 2018 <i>N</i> =66
Meteorological parameters			
Temperature, °C	5.9 ± 5.9 ((-7.5) – 16)	11 ± 3.8 (1.2 – 16)	1.9 ± 4.4 ((-7.5) – 11)
Relative humidity, %	35 ± 25 (7.1 – 99)	49 ± 26 (11 – 99)	23 ± 15 (7.1 – 67)
Gaseous pollutants, ppb			
SO ₂	3.2 ± 1.6 (1.1 – 7.9)	2.1 ± 0.8 (1.1 – 4.8)	4.3 ± 1.5 (2.2 – 7.9)

NO ₂	26 ± 13 (4.6 – 56)	25 ± 11 (4.6 – 43)	26 ± 14 (5.5 – 56)
NO	26 ± 28 (2.4 – 136)	28 ± 30 (2.4 – 136)	25 ± 26 (2.7 – 116)
CO	0.64 ± 0.55 (0.03 – 2.7)	0.81 ± 0.42 (0.12 – 1.6)	0.50 ± 0.61 (0.03 – 2.7)

Major components of PM _{2.5} , μg m ⁻³			
PM _{2.5}	65 ± 40 (6.1 – 195)	64 ± 39 (6.1 – 175)	66 ± 41 (8.6 – 195)
OC	8.3 ± 5.0 (0.99 – 26)	7.4 ± 3.9 (1.0 – 18)	9.1 ± 5.8 (1.8 – 26)
EC	4.7 ± 4.7 (0.11 – 25)	4.9 ± 3.8 (0.11 – 17)	4.5 ± 5.3 (0.18 – 25)
OC/EC	3.7 ± 3.6 (0.96 – 21)	2.7 ± 3.3 (0.96 – 21)	4.4 ± 3.7 (1.0 – 17)
SO ₄ ²⁻	4.8 ± 4.2 (0.85 – 25)	5.5 ± 3.5 (0.86 – 13)	4.3 ± 4.7 (0.85 – 25)
NO ₃ ⁻	11 ± 14 (0.09 – 58)	16 ± 16 (0.09 – 58)	6.8 ± 8.8 (0.29 – 37)
NH ₄ ⁺	4.7 ± 4.9 (0.02 – 20)	5.4 ± 5.4 (0.02 – 20)	4.2 ± 4.5 (0.19 – 20)
K ⁺	0.43 ± 0.39 (0.02 – 2.2)	0.38 ± 0.27 (0.03 – 1.1)	0.48 ± 0.46 (0.02 – 2.2)
Cl ⁻	1.5 ± 1.6 (0.06 – 9.2)	1.0 ± 0.98 (0.06 – 4.5)	1.9 ± 2.0 (0.13 – 9.2)

224

225

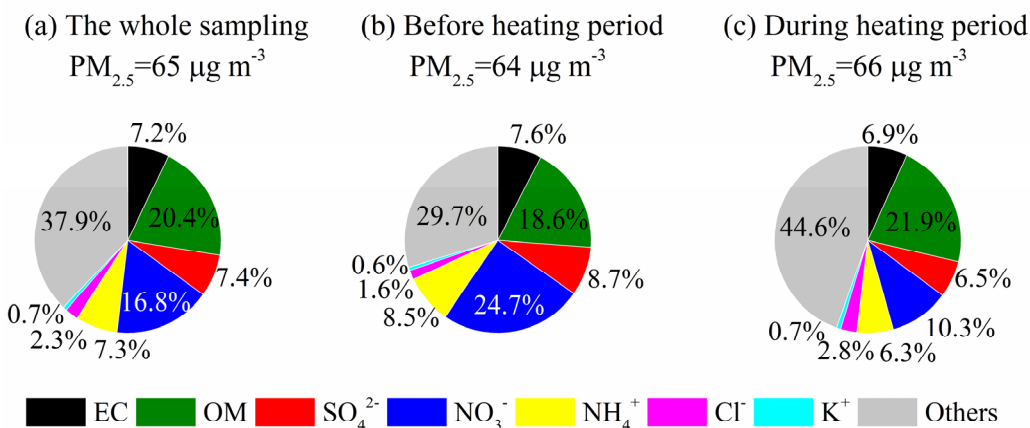


226

227

228 Fig.1 Time series of (a) RH and T, (b) SO₂ and NO₂, (c) PM_{2.5}, OM, and K⁺, (d) NACs
 229 and (e) OPAHs in the autumn and winter of urban Beijing. (Daytime is denoted by
 230 empty marks and the nighttime is represented by solid marks in the panel b–e. The
 231 pollution episodes, with elevated concentrations of daily PM_{2.5} more than 75 μg m⁻³ in
 232 two successive days, have been marked in light gray).

233



234

235

236

Fig.2 Chemical constitution of PM_{2.5} in the entire sampling period (a), before (b), and during (c) heating periods, respectively.

237

3.2 Concentration and composition variations of BrC compounds

238

This work quantified nine NACs and eight OPAHs. The corresponding

239

concentrations and compositions have been presented in Fig. 3 and Table S1

240

(supporting information).

241

As seen in Table S1, during the entire sampling, the total concentrations of NACs

242

($\sum 9\text{NACs}$) and their corresponding contribution to OM ($\sum 9\text{NACs}/\text{OM}$) respectively

243

averaged to 38 (1.2–263) ng m⁻³ and 0.25 (0.03–0.86) %. $\sum 9\text{NACs}$ and $\sum 9\text{NACs}/\text{OM}$

244

respectively averaged 53 (4.5–263) ng m⁻³ and 0.33 (0.09–0.86) % during heating, both

245

values are two times higher in magnitude in comparison to those measured before

246

heating (averaged 20 (1.2–108) ng m⁻³ and 0.15 (0.03–0.4) %, respectively). $\sum 9\text{NACs}$

247

exhibited a nighttime increase, reaching approximately twice the levels observed during

248

daytime throughout the entire campaign (Fig. 3a). The observed difference between day

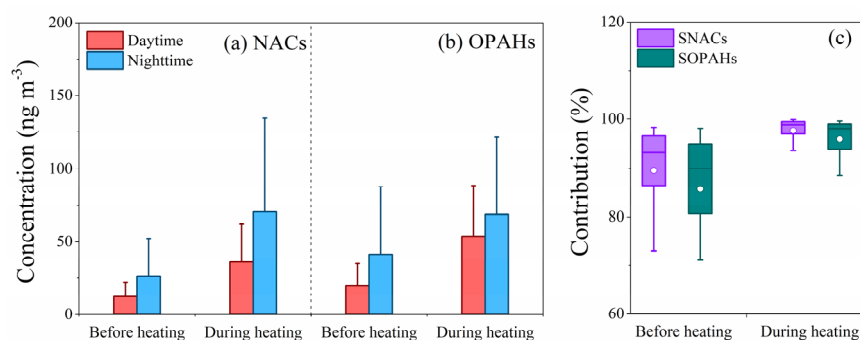
249

and night is consistent with our previous research (Ren et al., 2022). However, the

250

relative molecular composition of the total nine NACs in PM_{2.5} did not manifest any

251 significant change (Fig.4a, c), 4-Nitrophenol (4NP) was found to have the highest
252 concentration among all species, accounting for 44% and 42% of the total NACs before
253 and during heating, followed by 4-nitrocatechol (4NC) which accounted for 21% before
254 heating and 23% during heating. These findings align with the dominant species
255 observed in previous studies (Ren et al., 2022; Ren et al., 2023; Li et al., 2020b).
256 However, the values were much higher in comparison to those found in our earlier work
257 (Ren et al., 2022) at the same sample site during the spring ($8.6 (0.48-27) \text{ ng m}^{-3}$) and
258 summer ($8.5 (1.0-16) \text{ ng m}^{-3}$). It's plausible that seasonal variations in NACs are linked
259 to emission sources, formation pathways, and weather conditions. In this study, the
260 overall abundance of the $\Sigma 9\text{NACs}$ appeared to align closely with measurements from
261 earlier studies conducted during winter in Beijing ($74 \pm 51 \text{ ng m}^{-3}$ in winter, $20 \pm 12 \text{ ng}$
262 m^{-3} in autumn) (Li et al., 2020b) and Jinan ($48 \pm 26 \text{ ng m}^{-3}$ in winter, $9.8 \pm 4.2 \text{ ng m}^{-3}$
263 in autumn,) (Wang et al., 2018), but are significantly higher than those measured for
264 Xi'an ($17 \pm 12 \text{ ng m}^{-3}$) and Hong Kong ($12 \pm 14 \text{ ng m}^{-3}$) in winter (Wu et al., 2020;
265 Chow et al., 2015). In contrast to studies conducted abroad, the levels of $\Sigma 9\text{NACs}$ in
266 this particular study tended to be higher Germany showed 16 ng m^{-3} , while in the UK,
267 levels were around 19 ng m^{-3} . Belgium recorded levels of 32 ng m^{-3} in winter and 13
268 ng m^{-3} in autumn. (Teich et al., 2017; Mohr et al., 2013; Kahnt et al., 2013). This
269 indicates that it is urgent to further reduce the concentration of contaminant precursors
270 in China.

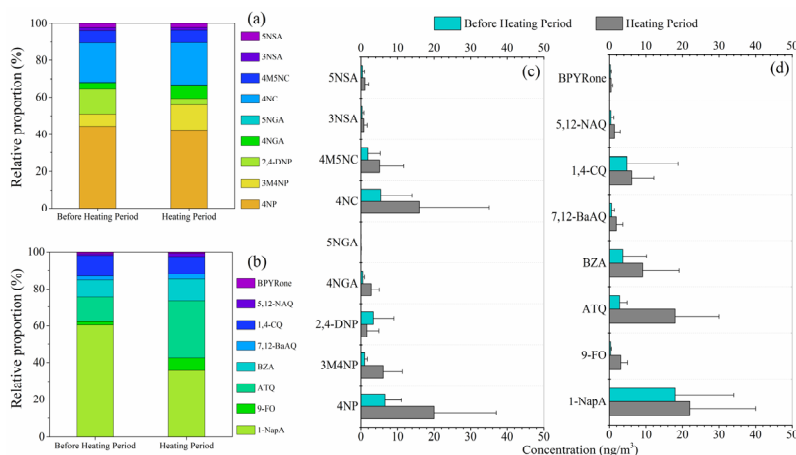


271

272 Fig.3 NACs and OPAHs concentrations (a,b) and contributions of secondary
 273 formation (SNACs, SOPAHs) to the total (c) before and during heating periods. The
 274 mean values are represented by the markers and the 25th and 75th percentiles are
 275 represented by whiskers.

276 Throughout the sampling, the total concentrations of OPAHs ($\sum 8\text{OPAHs}$)
 277 averaged 47 (1.2–234) ng m⁻³ whereas the mean value for their total contribution to OM
 278 ($\sum 8\text{OPAHs}/\text{OM}$) was 0.33 (0.06–0.81) % (Table S1). These values were both slightly
 279 higher than those of NACs in this work. $\sum 8\text{OPAHs}$ and $\sum 8\text{OPAHs}/\text{OM}$ respectively
 280 averaged 61 (6.9–218) ng m⁻³ and 0.40 (0.18–0.58) % during heating. These values are
 281 almost twice as much as those measured before heating (averaging 31 (2.1–234) ng m⁻³
 282 and 0.24 (0.06–0.81) %, respectively). Like the $\sum 9\text{NACs}$, the combined levels of
 283 $\sum 8\text{OPAHs}$ were higher during nighttime compared to daytime, averaging about twice
 284 as high before heating and 1.3 times during heating, as indicated in Fig. 3b. Among the
 285 eight OPAHs studied, 1-NapA constituted the highest proportion before (60%) and
 286 during (36%) heating. However, the relative proportion of ATQ more than doubled,
 287 increasing from 13% before heating to 31% during heating, as depicted in Fig. 4b and
 288 d. The average concentrations of $\sum 8\text{OPAHs}$ were higher than those recorded for other
 289 Chinese urban sites, including Guangzhou (23 ng m⁻³) and Xi'an (54 ng m⁻³) (Ren et
 290 al., 2017) as well as higher than those documented for the south (41.8 ng m⁻³, traffic

291 site) (Alves et al., 2017) and central ($\sim 10 \text{ ng m}^{-3}$) European cities (Lammel et al., 2020).
 292 The average concentrations of $\Sigma 8\text{OPAHs}$ were also higher than those recorded for
 293 Mainz, Germany ($0.047\text{-}1.6 \text{ ng m}^{-3}$) and Thessaloniki, Greece ($0.86\text{-}4.3 \text{ ng m}^{-3}$)
 294 (Kitanovski et al., 2020).



295 Fig.4 Comparison of measurements before and during the heating period at the urban
 296 site of Beijing, including (a) Relative proportion of NAC species, (b) Relative
 297 proportion of OPAH species, (c) NAC concentrations, and (d) OPAH concentrations.
 298 (4NP: 4-nitrophenol, 3M4NP: 3-methyl-4-nitrophenol, 2, 4-DNP: 2,4-dinitrophenol,
 299 4NGA: 4-nitroguaiacol, 5NGA: 5-nitroguaiacol, 4NC: 4-nitrocatechol, 4M5NC: 4-
 300 methyl-5-nitrocatechol, 3NSA: 3-nitro-salicylic acid, 5NSA: 5-nitro-salicylic acid; 1-
 301 NapA: 1-Naphthaldehyde, 9-FO: 9-fluorenone, ATQ: anthraquinone, BZA:
 302 benzanthrene, 7,12-BaAQ: benzo(a)anthracene-7,12-dione, 1,4-CQ: 1,4-
 303 chrysenequinone, 5,12-NAQ: 5,12-naphthacenequinone, and BPyRone: 6H-
 304 benzo(cd)pyrene-6-one)
 305

306 3.3 Sources and formation of BrC compounds

307 The relation between individual and total species and the associated pollutants—
 308 levoglucosan, K^+ , SO_2 , NO_2 , O_3 , RH, and SIA—was examined according to the data
 309 findings for the Pearson correlations shown in Table 2 (for NACs) and Table 3 (for
 310 OPAHs) to provide additional clarity regarding the source and formation of NACs and
 311 OPAHs. There were strong correlations between levoglucosan (an organic tracer

312 associated with biomass burning), K^+ (an inorganic tracer linked to biomass burning),
313 and NO_2 with total NACs and all identified NAC species, which indicated that both
314 automobile emissions and biomass burning played significant roles in the accumulation
315 of NACs in urban Beijing throughout the entire campaign. The correlation between
316 NACs and SO_2 was significantly higher during heating ($r=0.275$, $p<0.05$) compared to
317 pre-heating ($r=0.210$, $p>0.05$), suggesting that coal combustions play a more significant
318 role in NAC formation after heating commences.

319 In addition to these primary pollutants, NACs were also significantly correlated
320 with some secondary pollutants. Before heating, there existed a strong positive
321 association ($r=0.692$, $p<0.01$) between NACs and O_3 . However, this association
322 changed considerably after heating, becoming notably negative ($r=-0.303$, $p<0.05$). The
323 negative correlation between them may be related to the meteorological conditions
324 during the sampling period, e.g. lower temperature and weak solar irradiation, which
325 suppress the photo-degradation process of NACs (Li et al., 2020a). NACs and RH
326 concurrently displayed a strong positive correlation ($r=0.548$, $p<0.01$) during heating.
327 Along with SO_4^{2-} , NO_3^- , and NH_4^+ , total NACs also exhibited high positive correlation,
328 particularly while heating ($r=0.373$, $p<0.01$; $r=0.504$, $p<0.01$; $r=0.513$, $p<0.01$,
329 respectively). The overall concentrations of OPAHs and NACs throughout the
330 campaign exhibited substantial correlations ($r=0.830$, $p<0.01$ before heating; $r=0.895$,
331 $p<0.01$ during heating) (Table 3, Fig. S1). This suggests that their sources and/or
332 influencing variables were comparable. Specifically, throughout the entire campaign,
333 both total OPAHs and all identified OPAH species exhibited a strong correlation with

334 levoglucosan, K^+ , and NO_2 . This implies that automobile emissions and biomass
335 burning played significant roles as sources of OPAHs. OPAHs and SO_2 ($r=0.365$,
336 $p<0.01$) were determined to be more strongly correlated during heating than before
337 heating, suggesting the contribution of coal combustions to OPAHs becomes significant
338 during heating. Moreover, the correlation between OPAHs and O_3 was significantly
339 positive before heating ($r=0.563$, $p<0.01$), whereas it was significantly negative during
340 heating ($r=-0.385$, $p<0.01$). Furthermore, it was discovered that throughout the heating
341 phase, OPAHs and RH had a substantial positive correlation ($r=0.578$, $p<0.01$). Total
342 OPAHs also showed good correlations with SO_4^{2-} , NO_3^- , and NH_4^+ , especially during
343 heating period ($r=0.477$, $p<0.01$; $r=0.658$, $p<0.01$; $r=0.658$, $p<0.01$; respectively).

344 The observed phenomena, involving photooxidation before heating and aqueous
345 reactions during heating, strongly suggest a significant role in the secondary creation
346 of BrC throughout the entire sampling period. Earlier studies have highlighted that in
347 certain regions, the primary mechanism driving the formation of nitro-aromatic
348 hydrocarbons involves the gaseous phase oxidation of VOC precursors from
349 anthropogenic sources, such as toluene and benzene (Olariu et al., 2002; Sato et al.,
350 2007; Yuan et al., 2016; Ji et al., 2017; Liu et al., 2023). According to a recent study,
351 for instance, NACs are mostly generated at a rural location on China's Chongming
352 Island through gaseous-phase photooxidation (Liu et al., 2023). Aqueous reaction is
353 also a key pathway for the formation of BrC (Zhang et al., 2020; Cheng et al., 2021;
354 Jiang et al., 2023). Previous studies suggested that aqueous-phase reaction is an
355 important partant pathway for secondary BrC formation during the winter season

356 (Zhang et al., 2020; Li et al., 2020a). Wang et al.'s field observations in urban Beijing
 357 revealed that the aqueous reaction is a significant mechanism for the secondary
 358 synthesis of nitro-aromatic hydrocarbons during summer temperatures with high
 359 relative humidity (Wang et al., 2019). Furthermore, spherical primary OM particles (i.e.,
 360 tarballs), which are mainly from residential coal burning especially during heating
 361 period in the North China Plain, usually contain BrC species and their aqueous
 362 formation could occur during the long-range transport (Zhang et al., 2021a; Zhang et
 363 al., 2023).

Table 2 Correlations between NACs and meteorological parameters, gas pollutants, and aerosol components before (n=56) and during the heating period (n=66).

Before heating period	levoglucosan	K ⁺	SO ₂	NO ₂	O ₃	RH	SO ₄ ²⁻	NO ₃ ⁻	NH ₄ ⁺	
NACs	∑9NACs	0.897**	0.738**	0.210	0.714**	0.692**	0.170	0.359**	0.369**	0.190
	4NP	0.784**	0.699**	0.249	0.715**	0.649**	0.118	0.345**	0.372**	0.207
	3M4NP	0.752**	0.526**	0.290*	0.575**	0.511**	-0.011	0.184	0.191	0.029
	2,4-DNP	0.436**	0.353**	0.310*	0.463**	0.492**	-0.151	0.034	-0.048	-0.166
	4NGA	0.545**	0.361**	0.438**	0.560**	0.524**	-0.137	-0.016	-0.025	-0.131
	5NGA	0.582**	0.355**	0.114	0.343**	0.433**	0.005	0.120	0.139	0.044
	4NC	0.897**	0.748**	0.064	0.641**	0.617**	0.308*	0.448**	0.486**	0.325*
	4M5NC	0.885**	0.668**	0.076	0.579**	0.577**	0.252	0.364**	0.413**	0.261
	3NSA	0.791**	0.678**	0.129	0.553**	0.495**	0.214	0.457**	0.515**	0.331*
	5NSA	0.737**	0.596**	0.219	0.594**	0.553**	0.085	0.279*	0.316*	0.125
During heating period	levoglucosan	K ⁺	SO ₂	NO ₂	O ₃	RH	SO ₄ ²⁻	NO ₃ ⁻	NH ₄ ⁺	
NACs	∑9NACs	0.888**	0.786**	0.275*	0.481**	-0.303*	0.548**	0.373**	0.504**	0.513**
	4NP	0.812**	0.725**	0.262*	0.471**	-0.296*	0.586**	0.390**	0.489**	0.511**
	3M4NP	0.756**	0.655**	0.248	0.374**	-0.225	0.613**	0.318**	0.397**	0.462**
	2,4-DNP	0.537**	0.495**	0.280*	0.417**	-0.304*	0.199	0.136	0.247*	0.136
	4NGA	0.672**	0.406**	0.229	0.274*	-0.206	0.201	-0.047	0.074	0.081
	5NGA	0.275*	0.208	-0.028	0.190	0.026	-0.006	0.114	0.100	0.125
	4NC	0.894**	0.804**	0.248	0.454**	-0.290*	0.520**	0.378**	0.523**	0.530**
	4M5NC	0.882**	0.736**	0.246	0.434**	-0.244	0.430**	0.283*	0.421**	0.422**
	3NSA	0.788**	0.910**	0.348**	0.681**	-0.410**	0.577**	0.707**	0.888**	0.828**
	5NSA	0.820**	0.866**	0.268*	0.629**	-0.377**	0.599**	0.680**	0.846**	0.828**

**significant correlation at the 0.01 level;

*significant correlation at the 0.05 level;

364 From the above analysis, it is evident that there is a good correlation between these
365 two aromatic compounds and levoglucosan, as long-lived and inert chemicals in the
366 atmosphere (Cai et al., 2022). Therefore, it was not possible to determine with certainty
367 whether NACs and OPAHs originated predominantly from direct emission from the
368 biomass combustion or by secondary oxidation of the precursors produced as a result
369 of the process. Equations 1 and 2's outcomes indicated that in Beijing's urban areas
370 during fall and winter, NACs and OPAHs were predominantly of secondary origin.
371 Throughout the entire sampling period, secondary formation accounted for 17% to 99%
372 (average of 80%) of NACs and 8.9% to 99% (average of 73%) of OPAHs, as depicted
373 in Fig. 3c. Notably, the secondary fraction for OPAHs increased by 10.4% from 86% to
374 96%, while the secondary fraction for NACs rose by 8.9% from 90% before heating to
375 98% during heating. Earlier studies have highlighted the presence of significant levels
376 of secondary particle BrC during autumn and winter, particularly during haze periods
377 (Ding et al., 2017; Liu et al., 2023), and the results of this work corroborate well with
378 the earlier studies. Moreover, the good correlations between OPAHs and NACs with O₃
379 before heating and with RH during heating, confirm the importance of photochemical
380 and aqueous oxidation in these two different periods.

381

Table 3 Correlations between OPAHs and meteorological parameters, gas pollutants, and aerosol components before (n=56) and during the heating period (n=66).

Before heating period	Σ 9NACs	levoglucosan	K ⁺	SO ₂	NO ₂	O ₃	RH	SO ₄ ²⁻	NO ₃ ⁻	NH ₄ ⁺
Σ 8OPAHs	0.830**	0.865**	.605**	0.188	0.563**	0.563**	0.143	0.244	0.283*	0.139
OPAHs										
1-NapA	0.844**	0.870**	.621**	0.211	0.640**	0.622**	0.174	0.213	0.238	0.096
9-FO	0.775**	0.785**	.646**	0.283*	0.558**	0.573**	0.059	0.183	0.235	0.119
ATQ	0.633**	0.694**	.497**	0.392**	0.477**	0.483**	-0.018	0.042	0.061	-0.024

	BZA	0.686**	0.759**	.573**	0.232	0.537**	0.594**	0.110	0.177	0.206	0.117
	7,12-BaAQ	0.821**	0.865**	.685**	0.189	0.591**	0.622**	0.187	0.325*	0.356**	0.224
	1,4-CQ	0.636**	0.646**	.406**	0.041	0.303*	0.290*	0.102	0.259	0.309*	0.174
	5,12-NAQ	0.694**	0.752**	.563**	0.227	0.511**	0.559**	0.091	0.184	0.214	0.110
	BPYRone	0.827**	0.870**	.662**	0.131	0.590**	0.616**	0.226	0.345**	0.398**	0.255
	Heating period	Σ 9NACs	levoglucosan	K ⁺	SO ₂	NO ₂	O ₃	RH	SO ₄ ²⁻	NO ₃ ⁻	NH ₄ ⁺
	Σ 8OPAHs	0.895**	0.931**	0.877**	0.365**	0.678**	-0.385**	0.578**	0.477**	0.658**	0.658**
	1-NapA	0.752**	0.774**	0.659**	0.248	0.547**	-0.378**	0.332*	0.332**	0.498**	0.446**
	9-FO	0.478**	0.457**	0.342**	0.305*	0.302*	-0.020	0.131	-0.013	0.167	0.250*
	ATQ	0.780**	0.797**	0.815**	0.426**	0.668**	-0.372**	0.656**	0.466**	0.642**	0.684**
OPAHs	BZA	0.840**	0.881**	0.829**	0.332**	0.570**	-0.273*	0.577**	0.431**	0.568**	0.577**
	7,12-BaAQ	0.801**	0.856**	0.896**	0.391**	0.633**	-0.299*	0.655**	0.531**	0.689**	0.710**
	1,4-CQ	0.703**	0.780**	0.791**	0.244	0.597**	-0.282*	0.624**	0.560**	0.647**	0.675**
	5,12-NAQ	0.777**	0.818**	0.869**	0.365**	0.601**	-0.293*	0.535**	0.444**	0.619**	0.614**
	BPYRone	0.858**	0.857**	0.845**	0.339**	0.588**	-0.320*	0.478**	0.396**	0.612**	0.568**

**significant correlation at the 0.01 level;

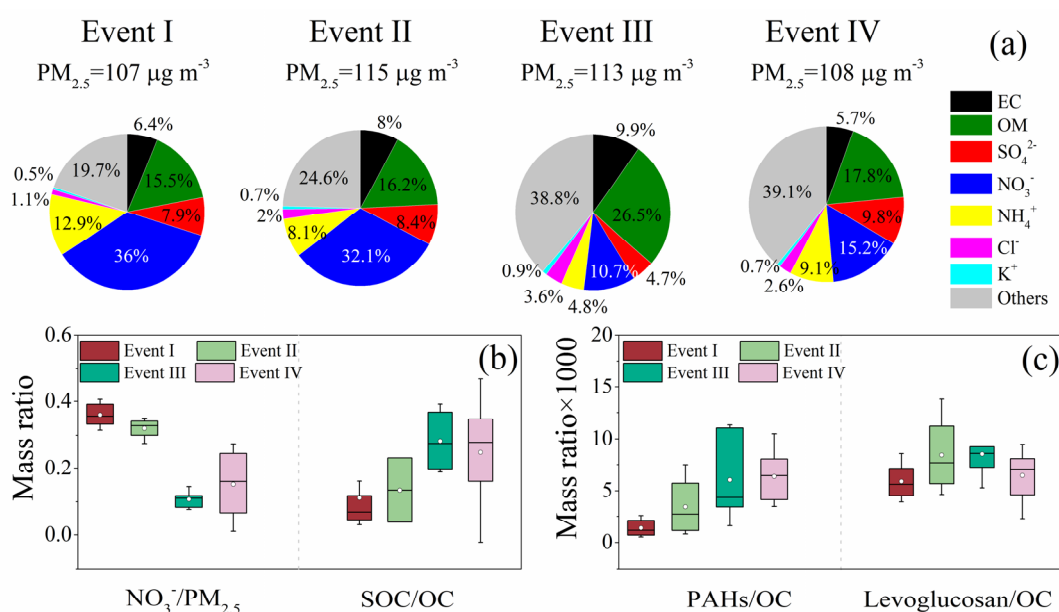
*significant correlation at the 0.05 level;

382

383 3.4 Different pollution characteristics in haze events

384 From Fig.1, it can be found that PM_{2.5} shows four equivalent maxima lasting for
385 two to five days. Among the four pollution events, two occurred before heating (24-27,
386 October and 5-6, November) and the other two occurred during heating (18-20,
387 November and 27-31 December). PM_{2.5} was significantly different in terms of its
388 chemical constituents before and during heating although the mass concentration of
389 PM_{2.5} was rather similar (respectively averaging 107, 115, 113, and 108 $\mu\text{g m}^{-3}$ for
390 Event I, II, III, and IV) (Fig. 5a). In the two events before heating, OM existed as the
391 second most dominant species in PM_{2.5}, with the respective relative abundance of 15.5%
392 and 16.2% in Events I and II. In contrast, OM surfaced as the most dominant species of
393 PM_{2.5} during heating. The relative abundance of OM (26.5%) during Event III was

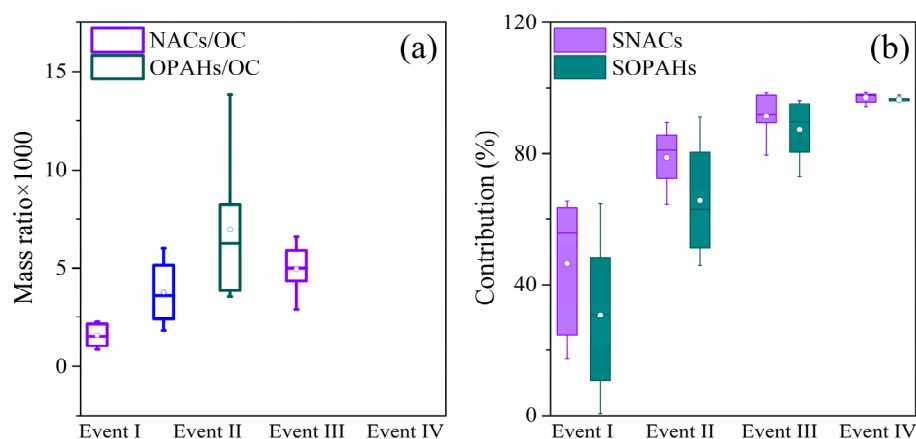
394 higher (17.8%) than that during Event IV (Fig.5a). The ratios of $\text{NO}_3^-/\text{PM}_{2.5}$ were higher
 395 in Events I and II as compared to Events III and IV, with the ratios of SOC/OC showing
 396 the opposite trend (Fig.5b), suggesting a significant increase in the concentration of
 397 secondary organic compounds after heating. In the context of fossil fuel combustion,
 398 PAHs serve as markers for coal burning, while levoglucosan acts as a significant tracer
 399 for biomass smoke. Figure 5c shows that the ratios of PAHs to organic carbon mass in
 400 $\text{PM}_{2.5}$ (PAHs/OC) were higher during Events III and IV compared to Events I and II.
 401 This underscores the heightened emissions from household burning of coal for heating
 402 purposes. Levoglucosan/OC, the mass ratio of levoglucosan to OC in $\text{PM}_{2.5}$, did not,
 403 however, rise considerably over the same period (Fig. 5c), indicating a similar degree
 404 of emissions from burning biomass before and during heating. This result was
 405 consistent with our earlier research from the 2014 APEC meeting (Wang et al., 2017).



406
 407 Fig.5 Comparative analysis of the chemical composition of $\text{PM}_{2.5}$ during four distinct
 408 events of air pollution. (a) Relative percentages of major species in $\text{PM}_{2.5}$; (b, c) mass
 409 ratios of the key species and organic tracers in $\text{PM}_{2.5}$. The mean values are represented
 410 by the markers and the 25th and 75th percentiles are represented by whiskers.

411 According to the majority of research, Beijing's haze is distinguished by intense
412 secondary formation (Zhang et al., 2018; Xu et al., 2017; Sun et al., 2016; Guo et al.,
413 2014). According to several research studies, organic materials (OM) predominates in
414 the autumn and winter, while secondary SIA is the most prevalent species in the
415 summer (Renhe et al., 2014). Additionally, according to a few investigators, SIA has a
416 major role in wintertime pollution episodes (Guo et al., 2014; Wang et al., 2016).
417 Furthermore, a recent investigation identified the species responsible for Beijing haze,
418 and listed distinct haze-driving species operative over the year: The haze is primarily
419 OM-driven during winter and late fall, nitrate-driven in early fall, sulfate-driven in
420 summer, whereas it is driven primarily by nitrates during spring (Tan et al., 2018). Table
421 4 and Fig.5a depict that PM_{2.5} was enriched with SIA especially NO₃⁻ during Events I
422 and II, but enriched OM with higher levels of SOC was observed during Events III and
423 IV. The findings strongly indicated that haze during fall and winter in urban Beijing
424 was primarily influenced by nitrate before heating and shifted to being driven by SOC
425 during heating. Table 4 illustrates that T and RH were notably higher during Events I
426 and II compared to Events III and IV. These warmer and moister conditions favored
427 photochemical oxidation, leading to an increased abundance of SIA during the same
428 period. Home heating activities, such as burning residential coal, were increased during
429 the heating period. This resulted in massive emissions of SO₂, NO_x, VOCs, and primary
430 particles, all of which were conducive to the generation of SOC. As a result, during
431 Events III and IV, SOC concentrations and relative abundances were higher than during
432 Events I and II. Furthermore, Fig. 6a shows that the NACs/OC and OPAHs/OC ratios

433 were significantly higher in Events III and IV compared to Events I and II. Figure 6b
 434 displays a parallel trend in the relative contributions of secondary formation for both
 435 events, highlighting a notable increase in the secondary formation of BrC during
 436 pollution events, particularly evident during heating periods.



437
 438 Fig. 6 Comparative analysis of the chemical composition of BrC during four distinct
 439 air pollution events. (a) Mass ratios of NACs and OPAHs to OC in PM_{2.5}. (b) Relative
 440 contributions of secondary formation (SNACs/OPAHs) to the total NACs/OPAHs in
 441 the fine particulate. The mean values are represented by the markers and the 25th and
 442 75th percentiles are represented by whiskers.

443

Table 4. Meteorological parameters, chemical components ($\mu\text{g m}^{-3}$) of PM_{2.5}, and concentrations of gaseous pollutants (ppb) among four pollution episodes in Beijing.

	Before Heating Period		During Heating Period	
	Event I 24/10–27/10 N=8	Event II 5/11–6/11 N=4	Event III 18/11–20/11 N=6	Event IV 27/12–31/12 N=10
PM _{2.5}	107 ± 29	115 ± 48	113 ± 37	108 ± 35
Temperature, °C	13 ± 1.6	8.8 ± 4.2	1.8 ± 2.6	1.8 ± 3.8
Relative humidity, %	79 ± 10	55 ± 26	29 ± 10	36 ± 22
SO ₂	1.4 ± 0.1	1.9 ± 1.1	5.0 ± 1.0	4.0 ± 1.2
NO	27 ± 19	27 ± 15	51 ± 42	47 ± 31
NO ₂	30 ± 6.7	33 ± 14	40 ± 12	37 ± 8.1
SIA ^a	62 ± 20	58 ± 22	23 ± 9.9	39 ± 30
NO ₃ ⁻	39 ± 13	38 ± 15	12 ± 5.2	18 ± 14
SOC ^b	1.9 ± 1.3	2.3 ± 1.8	7.0 ± 2.8	3.9 ± 2.5
NACs (ng m ⁻³)	17 ± 8.3	41 ± 36	131 ± 85	55 ± 27
OPAHs (ng m ⁻³)	21 ± 7.6	62 ± 85	127 ± 53	74 ± 23

^a SIA: secondary inorganic aerosols (the sum of sulfate, nitrate, and ammonium).

^b SOC: secondary organic carbon ($[SOC]=[OC]-[EC]\times([OC]/[EC])_{pri}$). $[OC]/[EC]_{pri}$ was estimated from the fitting of the minimum $[OC]/[EC]$ ratio, assuming that the primary source dominated the period with minimal secondary formation. In this work, $([OC]/[EC])_{pri}$ was estimated from the fitting of the lowest 15% $[OC]/[EC]$ ratios during the whole sampling period.

444 **4 Conclusions**

445 The current study determined the concentrations of PM_{2.5}-bound nine NACs and
446 eight OPAHs in autumn and winter in Beijing urban areas. The OPAHs and NACs
447 concentrations were much higher during heating than before heating. These species
448 have a distinct diurnal variation, with higher concentrations at night compared to day.
449 4-Nitrophenol, 4-nitrocatechol, and 1-Naphthaldehyde were the most abundantly
450 existing species in the whole campaign.

451 The primary sources of NACs and OPAHs were biomass combustion and
452 automobile emissions, with the secondary generation of BrC being the predominant
453 contributor across the entire sampling period. Our results underscore the significant role
454 of secondary generation in producing BrC, particularly its heightened contribution in
455 pollution events during heating. A comparative analysis of the chemical constitution of
456 PM_{2.5} and BrC in four different haze events also revealed that the haze was caused by
457 SOC during heating and by nitrate before heating in autumn and winter. Increased
458 attention should be directed towards reducing the emissions of aromatic hydrocarbons
459 and other anthropogenic volatile organic compounds (VOCs) when heating commences.
460 This focus is crucial for effectively mitigating pollution and ensuring the preservation
461 of human health. There is still only a limited volume of research on the molecular
462 makeup of BrC, and further research is needed to identify more impactful

463 chromophores at a molecular level. Additionally, a comprehensive exploration of the
464 secondary generation pathways and key influencing factors of BrC through field
465 observations and laboratory simulations is essential. This investigation is crucial for
466 accurately assessing the environmental and human health impacts of BrC.

467 **Data availability**

468 The field observational and the lab experimental data used in this study are
469 available from the corresponding author upon request (Hong Li via
470 lihong@craes.org.cn).

471 **Author contributions**

472 Yanqin Ren, Gehui Wang and Hong Li designed the research; Yanqin Ren,
473 Yuanyuan Ji and Zhenhai Wu collected the samples; Yanqin Ren, Fang Bi and Hao
474 Zhang conducted the experiments; Yanqin Ren and Gehui Wang analyzed the data,
475 Yanqin Ren wrote the paper; Gehui Wang, Junling Li, Haijie Zhang and Hong Li
476 contributed to the paper with useful scientific discussions and comments.

477 **Competing interests**

478 The authors declare that they have no conflict of interest.

479 **Acknowledgements**

480 This work was supported by the Fundamental Research Funds for Central Public
481 Welfare Scientific Research Institutes of China (No. 2022YSKY-27; No. 2019YSKY-
482 018), and the National Natural Science Foundation of China (No. 42130704; No.
483 41907197).

484 **References**

- 485 Alves, C., Vicente, A., CustÃ³dio, D., Cerqueira, M., Nunes, T., Pio, C., Lucarelli, F., Calzolari, G., Nava,
486 S., and Diapouli, E.: Polycyclic aromatic hydrocarbons and their derivatives (nitro-PAHs, oxygenated
487 PAHs, and azaarenes) in PM_{2.5} from Southern European cities, *Sci. Total. Environ.*, 595, 494-504,
488 <http://dx.doi.org/10.1016/j.scitotenv.2017.03.256>, 2017.
- 489 An, Z., Huang, R. J., Zhang, R., Tie, X., Li, G., Cao, J., Zhou, W., Shi, Z., Han, Y., Gu, Z., and Ji, Y.:
490 Severe haze in northern China: A synergy of anthropogenic emissions and atmospheric processes, *Proc*
491 *Natl Acad Sci U S A*, 116, 8657-8666, 10.1073/pnas.1900125116, 2019.
- 492 Bai, X., Wei, J., Ren, Y., Gao, R., Chai, F., Li, H., Xu, F., and Kong, Y.: Pollution characteristics and
493 health risk assessment of Polycyclic aromatic hydrocarbons and Nitrated polycyclic aromatic
494 hydrocarbons during heating season in Beijing, *JEnvS*, 123, 169-182,
495 <https://doi.org/10.1016/j.jes.2022.02.047>, 2023.
- 496 Cai, D., Wang, X., George, C., Cheng, T., Herrmann, H., Li, X., and Chen, J.: Formation of Secondary
497 Nitroaromatic Compounds in Polluted Urban Environments, *J. Geophys. Res.-Atmos.*,
498 <https://doi.org/10.1029/2021JD036167>, 2022.
- 499 Chen, Y., Zheng, P., Wang, Z., Pu, W., Tan, Y., Yu, C., Xia, M., Wang, W., Guo, J., Huang, D., Yan, C.,
500 Nie, W., Ling, Z., Chen, Q., Lee, S., and Wang, T.: Secondary Formation and Impacts of Gaseous Nitro-
501 Phenolic Compounds in the Continental Outflow Observed at a Background Site in South China, *Environ.*
502 *Sci. Technol.*, 56, 6933-6943, 10.1021/acs.est.1c04596, 2022.
- 503 Cheng, X., Chen, Q., Li, Y., Huang, G., Liu, Y., Lu, S., Zheng, Y., Qiu, W., Lu, K., Qiu, X., Bianchi, F.,
504 Yan, C., Yuan, B., Shao, M., Zhe Wang, R. M., Canagaratna, Zhu, T., Wu, Y., and Zeng, L.: Secondary
505 Production of Gaseous Nitrated Phenols in Polluted Urban Environments, *Environ. Sci. Technol.*, 55,
506 4410-4419, <https://doi.org/10.1021/acs.est.0c07988>, 2021.
- 507 Chow, K. S., Huang, X. H. H., and Yu, J. Z.: Quantification of nitroaromatic compounds in atmospheric
508 fine particulate matter in Hong Kong over 3 years: field measurement evidence for secondary formation
509 derived from biomass burning emissions, *Environmental Chemistry*, 13, 665,
510 <https://doi.org/10.1071/EN15174>, 2015.
- 511 Claeys, M., Vermeulen, R., Yasmeen, F., Gómez-González, Y., Chi, X., Maenhaut, W., Mészáros, T., and

512 Salma, I.: Chemical characterisation of humic-like substances from urban, rural and tropical biomass
513 burning environments using liquid chromatography with UV/vis photodiode array detection and
514 electrospray ionisation mass spectrometry, *Environmental Chemistry*, 9, 273-284, 2012.

515 Ding, X., Zhang, Y. Q., He, Q., Yu, Q. Q., Wang, J. Q., Shen, R. Q., Song, W., Wang, Y., and Wang, X.:
516 Significant increase of aromatics-derived secondary organic aerosol during fall to winter in China,
517 *Environ. Sci. Technol.*, 13, 7432-7441, <http://doi.org/10.1021/acs.est.6b06408>, 2017.

518 Du, Z., He, K., Cheng, Y., Duan, F., Ma, Y., Liu, J., Zhang, X., Zheng, M., and Weber, R.: A yearlong
519 study of water-soluble organic carbon in Beijing II: Light absorption properties, *Atmos. Environ.*, 89,
520 235-241, <http://doi.org/10.1016/j.atmosenv.2014.02.022>, 2014.

521 Fan, Xingjun, Peng, Ping'an, Song, and Jianzhong: Temporal variations of the abundance and optical
522 properties of water soluble Humic-Like Substances (HULIS) in PM2.5 at Guangzhou, China, *Atmos.*
523 *Res.*, <http://doi.org/10.1016/j.atmosres.2015.12.024>, 2016.

524 Finewax, Zachary, de, Gouw, Joost, A., Ziemann, Paul, and J.: Identification and Quantification of 4-
525 Nitrocatechol Formed from OH and NO₃ Radical-Initiated Reactions of Catechol in Air in the Presence
526 of NO_x: Implications for Secondary Organic Aerosol Formation from Biomass Burning, *Environ. Sci.*
527 *Technol.*, <http://doi.org/10.1021/acs.est.7b05864> 2018.

528 Guo, S., Hu, M., Zamora, M. L., Peng, J., Shang, D., Zheng, J., Du, Z., Wu, Z., Shao, M., and Zeng, L.:
529 Elucidating severe urban haze formation in China, *Proc. Natl. Acad. Sci. USA.*, 111, 17373-17378,
530 <http://doi.org/10.1073/pnas.1419604111>, 2014.

531 Huang, R. J., Yang, L., Cao, J., Chen, Y., Chen, Q., Li, Y., Duan, J., Zhu, C., Dai, W., Wang, K., Lin, C.,
532 Ni, H., Corbin, J. C., Wu, Y., Zhang, R., Tie, X., Hoffmann, T., O'Dowd, C., and Dusek, U.: Brown
533 Carbon Aerosol in Urban Xi'an, Northwest China: The Composition and Light Absorption Properties,
534 *Environ. Sci. Technol.*, 52, 6825-6833, <http://doi.org/10.1021/acs.est.8b02386>, 2018.

535 Iinuma, Y., Boge, O., Graefe, R., and Herrmann, H.: Methyl-Nitrocatechols: Atmospheric Tracer
536 Compounds for Biomass Burning Secondary Organic Aerosols, *Environ. Sci. Technol.*, 44, 8453,
537 <http://doi.org/10.1021/es102938a>, 2010.

538 Ji, Y., Zhao, J., Terazono, H., Misawa, K., and Zhang, R.: Reassessing the atmospheric oxidation
539 mechanism of toluene, *Proc Natl Acad Sci U S A*, 114, <http://doi.org/10.1073/pnas.1705463114>, 2017.

540 Jiang, H., Cai, J., Feng, X., Chen, Y., Wang, L., Li, J., Tang, J., Mo, Y., Zhang, X., Zhang, G., Mu, Y.,
541 and Chen, J.: Aqueous-Phase Secondary Processes and Meteorological Change Promote the Brown
542 Carbon Formation and Transformation During Haze Events, *J. Geophys. Res.-Atmos.*,
543 <http://doi.org/10.1029/2023JD038735>, 2023.

544 Kahnt, A., Behrouzi, S., Vermeylen, R., Shalamzari, M. S., Vercauteren, J., Roekens, E., Claeys, M., and
545 Maenhaut, W.: One-year study of nitro-organic compounds and their relation to wood burning in PM10
546 aerosol from a rural site in Belgium, *Atmos. Environ.*, 81, 561-568,
547 <http://dx.doi.org/10.1016/j.atmosenv.2013.09.041>, 2013.

548 Kitanovski, Z., Shahpoury, P., Samara, C., Voliotis, A., and Lammel, G.: Composition and mass size
549 distribution of nitrated and oxygenated aromatic compounds in ambient particulate matter from southern
550 and central Europe – implications for the origin, *Atmos. Chem. Phys.*, 20, 2471-2487,
551 <https://doi.org/10.5194/acp-20-2471-2020>, 2020.

552 Lammel, G., Kitanovski, Z., Kukucka, P., Novák, J., and Wietzoreck, M.: Oxygenated and nitrated
553 polycyclic aromatic hydrocarbons (OPAHs, NPAHs) in ambient air - levels, phase partitioning, mass size
554 distributions and inhalation bioaccessibility, *Environ. Sci. Technol.*, 54, 2615-2625,

555 <https://dx.doi.org/10.1021/acs.est.9b06820>, 2020.

556 Laskin, A., Laskin, J., and Nizkorodov, S. A.: Chemistry of atmospheric brown carbon, *Chem. Rev.*, 115,
557 4335-4382, <http://doi.org/10.1021/cr5006167>, 2015.

558 Li, J., Wang, G., Ren, Y., Wang, J., Wu, C., Han, Y., Zhang, L., Cheng, C., and Meng, J.: Identification
559 of chemical compositions and sources of atmospheric aerosols in Xi'an, inland China during two types
560 of haze events, *Sci. Total. Environ.*, 566, 230-237, <http://dx.doi.org/10.1016/j.scitotenv.2016.05.057>,
561 2016.

562 Li, J., Zhang, Q., Wang, G., Li, J., Wu, C., Liu, L., Wang, J., Jiang, W., Li, L., Ho, K. F., and Cao, J.:
563 Optical properties and molecular compositions of water-soluble and water-insoluble brown carbon (BrC)
564 aerosols in Northwest China, *Atmos. Chem. Phys.*, 20, 4889–4904, [https://doi.org/10.5194/acp-20-4889-](https://doi.org/10.5194/acp-20-4889-2020)
565 [2020](https://doi.org/10.5194/acp-20-4889-2020), 2020a.

566 Li, X., Yang, Y., Liu, S., Zhao, Q., Wang, G., and Wang, Y.: Light absorption properties of brown carbon
567 (BrC) in autumn and winter in Beijing: Composition, formation and contribution of nitrated aromatic
568 compounds, *Atmos. Environ.*, 223, 117289, <https://doi.org/10.1016/j.atmosenv.2020.117289>, 2020b.

569 Li, X., Han, J., Hopke, P. K., Hu, J., Shu, Q., Chang, Q., and Ying, Q.: Quantifying primary and secondary
570 humic-like substances in urban aerosol based on emission source characterization and a source-oriented
571 air quality model, Copernicus GmbH, <https://doi.org/10.5194/acp-19-2327-2019>, 2019.

572 Li, Y., Bai, X., Ren, Y., Gao, R., Ji, Y., Wang, Y., and Li, H.: PAHs and nitro-PAHs in urban Beijing from
573 2017 to 2018: Characteristics, sources, transformation mechanism and risk assessment, *J. Hazard. Mater.*,
574 436, 1-11, <https://doi.org/10.1016/j.jhazmat.2022.129143>, 2022.

575 Liu, J., Mo, Y., Ding, P., Li, J., Shen, C., and Zhang, G.: Dual carbon isotopes (^{14}C and ^{13}C) and optical
576 properties of WSOC and HULIS-C during winter in Guangzhou, China, *Sci. Total. Environ.*, 633, 1571-
577 1578, <https://doi.org/10.1016/j.scitotenv.2018.03.293>, 2018.

578 Liu, X., Wang, H., Wang, F., Lv, S., Wu, C., Zhao, Y., Zhang, S., Liu, S., Xu, X., Lei, Y., and Wang, G.:
579 Secondary Formation of Atmospheric Brown Carbon in China Haze: Implication for an Enhancing Role
580 of Ammonia, *Environ. Sci. Technol.*, <http://doi.org/10.1021/acs.est.3c03948>, 2023.

581 Lu, C., Wang, X., Dong, S., Zhang, J., and Wang, W.: Emissions of fine particulate nitrated phenols from
582 various on-road vehicles in China, *Environ. Res.*, 179, 108709,
583 <https://doi.org/10.1016/j.envres.2019.108709>, 2019a.

584 Lu, C., Wang, X., Li, R., Gu, R., Zhang, Y., Li, W., Gao, R., Chen, B., Xue, L., and Wang, W.: Emissions
585 of fine particulate nitrated phenols from residential coal combustion in China, *Atmos. Environ.*, 203, 10-
586 17, <https://doi.org/10.1016/j.atmosenv.2019.01.047>, 2019b.

587 Ma, Y., Cheng, Y., Qiu, X., Cao, G., Fang, Y., Wang, J., Zhu, T., Yu, J., and Hu, D.: Sources and oxidative
588 potential of water-soluble humic-like substances (HULISWS) in fine particulate matter (PM_{2.5}) in
589 Beijing, *Atmos. Chem. Phys.*, 18, 5607–5617, <https://doi.org/10.5194/acp-18-5607-2018>, 2018.

590 Mohr, C., Lopez-Hilfiker, F. D., Zotter, P., A. S. H. P., Xu, L., Ng, N. L., Herndon, S. C., Williams, L.
591 R., Franklin, J. P., Zahniser, M. S., Worsnop, D. R., Knighton, W. B., Aiken, A. C., Gorkowski, K. J.,
592 Dubey, M. K., Allan, J. D., and Thornton, J. A.: Contribution of Nitrated Phenols to Wood Burning Brown
593 Carbon Light Absorption in Detling, United Kingdom during Winter Time, *Environ. Sci. Technol.*, 47,
594 6316-6324, <https://doi.org/10.1021/es400683v>, 2013.

595 Ni, H., Huang, R. J., Pieber, S. M., Corbin, J. C., and Dusek, U.: Brown Carbon in Primary and Aged
596 Coal Combustion Emission, *Environ. Sci. Technol.*, 55, 5701-5710,
597 <https://doi.org/10.1021/acs.est.0c08084>, 2021.

598 Olariu, R. I., Klotz, B. R., Barnes, I., Becker, K. H., and Mocanu, R.: FT-IR study of the ring-retaining
599 products from the reaction of OH radicals with phenol, o-, m-, and p-cresol, *Atmos. Environ.*, 36, 3685-
600 3697, [http://doi.org/10.1016/S1352-2310\(02\)00202-9](http://doi.org/10.1016/S1352-2310(02)00202-9), 2002.

601 Ren, Y., Wang, G., Wei, J., Tao, J., Zhang, Z., and Li, H.: Contributions of primary emissions and
602 secondary formation to nitrated aromatic compounds in themountain background region of Southeast
603 China, *Atmos. Chem. Phys.*, 23, 6835-6848, <http://doi.org/10.5194/acp-23-6835-2023>, 2023.

604 Ren, Y., Wei, J., Wang, G., Wu, Z., Ji, Y., and Li, H.: Evolution of aerosol chemistry in Beijing under
605 strong influence of anthropogenic pollutants: Composition, sources, and secondary formation of fine
606 particulate nitrated aromatic compounds, *Environ. Res.*, 204, 111982,
607 <https://doi.org/10.1016/j.envres.2021.111982>, 2022.

608 Ren, Y., Wei, J., Wu, Z., Ji, Y., Bi, F., Gao, R., Wang, X., Wang, G., and Li, H.: Chemical components
609 and source identification of PM_{2.5} in non-heating season in Beijing: The influences of biomass burning
610 and dust, *Atmos. Res.*, 105412, <https://doi.org/10.1016/j.atmosres.2020.105412>, 2021.

611 Ren, Y., Zhou, B., Tao, J., Cao, J., Zhang, Z., Wu, C., Wang, J., Li, J., Zhang, L., Han, Y., Liu, L., Cao,
612 C., and Wang, G.: Composition and size distribution of airborne particulate PAHs and oxygenated PAHs
613 in two Chinese megacities, *Atmos. Res.*, 183, 322-330, <https://doi.org/10.1016/j.atmosres.2020.105412>,
614 2017.

615 Renhe, Z., Qiang, L. I., and Ruonan, Z.: Meteorological conditions for the persistent severe fog and haze
616 event over eastern China in January 2013, *Science China-earth Sciences*, 57, 26-35,
617 <http://doi.org/10.1007/s11430-013-4774-3>, 2014.

618 Sato, K., Hatakeyama, S., and Imamura, T.: Secondary Organic Aerosol Formation during the
619 Photooxidation of Toluene: NO_x Dependence of Chemical Composition, *J. Phys. Chem. A*, 111,
620 <http://doi.org/10.1021/jp071419f>, 2007.

621 Song, J., Li, M., and Zou, C.: Molecular characterization of nitrogen-containing compounds in humic-
622 like substances emitted from biomass burning and coal combustion, *Environ. Sci. Technol.*, 56, 119-130,
623 <https://doi.org/10.1021/acs.est.1c04451>, 2022.

624 Song, J., Zhu, M., Wei, S., Peng, P. A., and Ren, M.: Abundance and 14C-based source assessment of
625 carbonaceous materials in PM_{2.5} aerosols in Guangzhou, South China, *Atmos. Pollut. Res.*, 10, 313-320,
626 <https://doi.org/10.1016/j.apr.2018.09.003>, 2018.

627 Sun, Y., Du, W., Fu, P., Wang, Q., Li, J., Ge, X., Zhang, Q., Zhu, C., Ren, L., and Xu, W.: Primary and
628 secondary aerosols in Beijing in winter: sources, variations and processes, *Atmos. Chem. Phys.*, 16,
629 8309-8329, <http://doi.org/10.5194/acp-16-8309-2016>, 2016.

630 Sun, Y. L., Wang, Z. F., Fu, P. Q., Yang, T., Jiang, Q., Dong, H. B., Li, J., and Jia, J. J.: Aerosol
631 composition, sources and processes during wintertime in Beijing, China, *Atmos. Chem. Phys.*, 13, 4577-
632 4592, <http://doi.org/10.5194/acp-13-4577-2013>, 2013.

633 Tan, J., Xiang, P., Zhou, X., Duan, J., Ma, Y., He, K., Cheng, Y., Yu, J., and Querol, X.: Chemical
634 characterization of humic-like substances (HULIS) in PM_{2.5} in Lanzhou, China, *Sci. Total. Environ.*,
635 573, 1481-1490, <http://dx.doi.org/10.1016/j.scitotenv.2016.08.025>, 2016.

636 Tan, T., Hu, M., Li, M., Guo, Q., Wu, Y., Fang, X., Gu, F., Wang, Y., and Wu, Z.: New insight into PM_{2.5}
637 pollution patterns in Beijing based on one-year measurement of chemical compositions, *Sci. Total.*
638 *Environ.*, 621, 734-743, <https://doi.org/10.1016/j.scitotenv.2017.11.208>, 2018.

639 Teich, M., Pinxteren, D. V., Kecorius, S., Wang, Z., Herrmann, H. J. E. S., and Technology: First
640 Quantification of Imidazoles in Ambient Aerosol Particles: Potential Photosensitizers, *Brown Carbon*

641 Constituents, and Hazardous Components, 50, 1166-1173, <http://doi.org/10.1021/acs.est.5b05474> 2016.

642 Teich, M., Van Pinxteren, D., Wang, M., Kecorius, S., Wang, Z., Müller, T., Mocnik, G., and Herrmann,
643 H.: Contributions of nitrated aromatic compounds to the light absorption of water-soluble and particulate
644 brown carbon in different atmospheric environments in Germany and China, *Atmos. Chem. Phys.*, 17,
645 1653-1672, <https://doi.org/10.5194/acp-17-1653-2017>, 2017.

646 Wang, G., Kawamura, K., Xie, M., Hu, S., Gao, S., Cao, J., An, Z., and Wang, Z.: Size-distributions of
647 n-alkanes, PAHs and hopanes and their sources in the urban, mountain and marine atmospheres over East
648 Asia, *Atmos. Chem. Phys.*, 9, 8869-8882, <http://doi.org/10.5194/acp-9-8771-2009>, 2009.

649 Wang, G., Zhang, R., Gomez, M. E., Yang, L., Levy, Z. M., Hu, M., Lin, Y., Peng, J., Guo, S., and Meng,
650 J.: Persistent sulfate formation from London Fog to Chinese haze, *Proc Natl Acad Sci U S A*, 113, 13630-
651 13635, <https://doi.org/10.1073/pnas.1616540113>, 2016.

652 Wang, H., Gao, Y., Wang, S., Wu, X., Liu, Y., Li, X., Dandan, Huang, Lou, S., Wu, Z., Guo, S., Jing, S.,
653 Li, Y., Huang, C., Tyndall, G. S., Orlando, J. J., and Zhang, X.: Atmospheric Processing of Nitrophenols
654 and Nitrocresols From Biomass Burning Emissions, *J. Geophys. Res.-Atmos.*, 125,
655 <http://doi.org/10.1029/2020JD033401>, 2020a.

656 Wang, J., Wang, G., Gao, J., Wang, H., Ren, Y., Li, J., Zhou, B., Wu, C., Zhang, L., Wang, S., and Chai,
657 F.: Concentrations and stable carbon isotope compositions of oxalic acid and related SOA in Beijing
658 before, during, and after the 2014 APEC, *Atmos. Chem. Phys.*, 17, 981-992,
659 <http://doi.org/doi:10.5194/acp-17-981-2017>, 2017.

660 Wang, L., Wang, X., Gu, R., Hao, W., and Wang, W.: Observations of fine particulate nitrated phenols in
661 four sites in northern China: concentrations, source apportionment, and secondary formation, *Atmos.*
662 *Chem. Phys.*, 1-24, <https://doi.org/10.5194/acp-18-4349-2018>, 2018.

663 Wang, Y., Hu, M., Li, X., and Xu, N.: Chemical Composition, Sources and Formation Mechanisms of
664 Particulate Brown Carbon in the Atmosphere (in Chinese), *Progress in Chemistry*, 32, 627-645,
665 <http://doi.org/10.7536/PC190917>, 2020b.

666 Wang, Y., Hu, M., Wang, Y., Zheng, J., and Yu, J. Z.: The formation of nitro-aromatic compounds under
667 high NO_x and anthropogenic VOC conditions in urban Beijing, China, *Atmos. Chem. Phys.*, 19, 7649-
668 7665, <https://doi.org/10.5194/acp-19-7649-2019>, 2019.

669 Wang, Y., Mehra, A., Krechmer, J. E., Yang, G., and Wang, L.: Oxygenated products formed from OH-
670 initiated reactions of trimethylbenzene: Autoxidation and accretion, *Atmos. Chem. Phys.*, 20, 9563-9579,
671 <https://doi.org/10.5194/acp-20-9563-2020>, 2020c.

672 Wu, C., Wang, G., Li, J., Li, J., Cao, C., Ge, S., Xie, Y., Chen, J., Li, X., Xue, G., Wang, X., Zhao, Z.,
673 and Cao, F.: The characteristics of atmospheric brown carbon in Xi'an, inland China: sources, size
674 distributions and optical properties, *Atmos. Chem. Phys.*, 20, 2017-2030, [https://doi.org/10.5194/acp-20-](https://doi.org/10.5194/acp-20-2017-2020)
675 [2017-2020](https://doi.org/10.5194/acp-20-2017-2020), 2020.

676 Xie, M., Chen, X., Hays, M., Lewandowski, M., Offenberg, J. H., Kleindienst, T. E., and Holder, A. L.:
677 Light Absorption of Secondary Organic Aerosol: Composition and Contribution of Nitroaromatic
678 Compounds, *Environmental Science & Technology*, 51, 11607-11616,
679 <https://doi.org/10.1021/acs.est.7b03263>, 2017.

680 Xu, L., Duan, F., He, K., Ma, Y., Zhu, L., Zheng, Y., Huang, T., Kimoto, T., Ma, T., and Li, H.:
681 Characteristics of the secondary water-soluble ions in a typical autumn haze in Beijing, *Environ. Pollut.*,
682 227, 296-305, <http://dx.doi.org/10.1016/j.envpol.2017.04.076>, 2017.

683 Yan, J., Wang, X., Gong, P., Wang, C., and Cong, Z.: Review of brown carbon aerosols: Recent progress

684 and perspectives, *Sci. Total. Environ.*, 634, 1475-1485, <https://doi.org/10.1016/j.scitotenv.2018.04.083>,
685 2018.

686 Yuan, B., Liggió, J., Wentzell, J., Li, S. M., and Stark, H.: Secondary formation of nitrated phenols:
687 insights from observations during the Uintah Basin Winter Ozone Study (UBWOS) 2014, *Atmos. Chem.*
688 *Phys.*, 16, <http://doi.org/10.5194/acp-16-2139-2016>, 2016.

689 Zhang, J., Li, W., Wang, Y., Teng, X., Zhang, Y., Xu, L., Yuan, Q., Wu, G., Niu, H., and Shao, L.:
690 Structural Collapse and Coating Composition Changes of Soot Particles During Long-Range Transport,
691 *J. Geophys. Res.-Atmos.*, 128, 10.1029/2023jd038871, 2023.

692 Zhang, J., Yuan, Q., Liu, L., Wang, Y., Zhang, Y., Xu, L., Pang, Y., Zhu, Y., Niu, H., Shao, L., Yang, S.,
693 Liu, H., Pan, X., Shi, Z., Hu, M., Fu, P., and Li, W.: Trans-Regional Transport of Haze Particles From
694 the North China Plain to Yangtze River Delta During Winter, *J. Geophys. Res.-Atmos.*, 126,
695 10.1029/2020jd033778, 2021a.

696 Zhang, Q., Shen, Z., Zhang, L., Zeng, Y., and Cao, J. J.: Investigation of Primary and Secondary
697 Particulate Brown Carbon in Two Chinese Cities of Xi'an and Hong Kong in Wintertime, *Environ. Sci.*
698 *Technol.*, 54, 3803-3813, <http://doi.org/10.1021/acs.est.9b05332>, 2020.

699 Zhang, R., Sun, X., Huang, Y., Shi, A., Yan, J., Nie, T., Yan, X., and Li, X.: Secondary inorganic aerosols
700 formation during haze episodes at an urban site in Beijing, China, *Atmos. Environ.*, 177, 275-282,
701 <https://doi.org/10.1016/j.atmosenv.2017.12.031>, 2018.

702 Zhang, R., Wang, G., Guo, S., L.Zamora, M., Ying, Q., Lin, Y., Wang, W., Hu, M., and Wang, Y.:
703 Formation of Urban Fine Particulate Matter, *Chem. Rev.*, 115, 3803-3855, 2015.

704 Zhang, W., Wang, W., Li, J., Ma, S., and Ge, M.: Light absorption properties and potential sources of
705 brown carbon in Fenwei Plain during winter 2018–2019, *JEnvS*, 102, 53-63,
706 <https://doi.org/10.1016/j.jes.2020.09.007>, 2021b.

707 Zhao, M., Qiao, T., Li, Y., Tang, X., Xiu, G., and Yu, J.: Temporal variations and source apportionment
708 of Hulis-C in PM_{2.5} in urban Shanghai, *Sci. Total. Environ.*, 571, 18-26,
709 <http://doi.org/10.1016/j.scitotenv.2016.07.127>, 2016.

710 Zhu, C. S., Qu, Y., Zhou, Y., Huang, H., and Cao, J. J.: High light absorption and radiative forcing
711 contributions of primary brown carbon and black carbon to urban aerosol, *Gondwana Res*, 90, 159-164,
712 <https://doi.org/10.1016/j.gr.2020.10.016>, 2021.

713